

# Multimodality imaging of the orbit

Pradipta C Hande, Inder Talwar<sup>1</sup>

Department of Radiodiagnosis and Imaging, INHS Asvini, Colaba, <sup>1</sup>Department of Radiodiagnosis, Bombay Hospital Institute of Medical Sciences, Marine Lines, Mumbai, India

**Correspondence:** Dr. Pradipta C Hande, Department of Radiodiagnosis and Imaging, INHS Asvini, Colaba, Mumbai - 400 005, India.  
E-mail: pradipta.hande@gmail.com

## Abstract

The role of imaging is well established in the evaluation of orbital diseases. Ultrasonography, Computed tomography and Magnetic resonance imaging are complementary modalities, which allow direct visualization of regional anatomy, accurate localization and help to characterize lesions to make a reliable radiological diagnosis. The purpose of this pictorial essay is to highlight the imaging features of commonly encountered pathologies which involve the orbit.

**Key words:** Imaging; magnetic resonance imaging; multidetector computed tomography; orbit

## Introduction

The orbit is the site of a large number of pathologies of diverse etiologies, and imaging has to be tailored to the symptoms and clinical findings. The commonest clinical indications for orbital imaging are proptosis/exophthalmos, diminished vision, enophthalmos, diplopia, leucocoria, pain, tumor and trauma. It is also used for evaluation in craniofacial developmental anomalies and epiphora.

### Relevant anatomy

Good knowledge of detailed anatomy of the orbits and its contents is essential to evaluate orbital pathologies.<sup>[1,2]</sup> The orbits are pyramidal shaped bony cavities with the base anteriorly (orbital opening). The rigid bony orbital walls are formed by seven bones namely frontal, sphenoid, ethmoid, lacrimal, maxilla, zygoma, and the palatine. The orbits are surrounded by air containing paranasal sinuses and nasal cavity medially. The lateral wall is thickest formed by the greater wing of sphenoid and frontal process of the zygomatic bone. The orbital roof separates it from the anterior cranial fossa superiorly and the floor is formed by the roof of the maxillary antrum which is relatively thin. Medially, the orbit

is separated from the ethmoidal air cells by a very thin orbital plate of ethmoid (lamina papyracea). The walls of the orbit are vulnerable to fractures due to head injuries and facial trauma.

The main contents of the orbit include globe/eyeball, seven extraocular muscles (EOM), blood vessels, cranial nerves (II with meninges, III, IV, V, VI), sympathetic and parasympathetic nerves, lacrimal gland and apparatus surrounded by fat and connective tissue. The optic canal, superior and inferior orbital fissure are apertures that transmit vital nerves and vessels to and from the orbit and brain at the orbital apex. The tendinous ring (annulus) of Zinn is the common origin of the EOM including the medial rectus (MR), lateral rectus (LR), superior rectus (SR) except inferior rectus (IR). The four recti attach anteriorly onto the globe forming a muscle cone tapering towards the apex, which divides the orbit into intraconal, conal, extraconal compartments<sup>[3]</sup> and are well identified on imaging. This descriptive approach is useful in localizing the lesions of the orbit to a specific compartment, thereby helping in the diagnosis and further planning the surgery. The orbital walls lined by the periosteum (periorbita) have potential extraperiosteal and subperiosteal spaces.

The orbits are closely related anatomically to the adjacent paranasal sinuses, pterygopalatine fossa,<sup>[1]</sup> and cerebral contents making them vulnerable to extension of disease processes involving these structures.

### Imaging considerations

The inherent soft tissue contrast of the fluid-filled globe, retrobulbar contents within the fat and bony walls of the

#### Access this article online

##### Quick Response Code:



Website:  
www.ijri.org

DOI:  
10.4103/0971-3026.107184

orbits delineates the orbital anatomy well [Figures 1 and 2]. Ultrasonography (USG) (B-scan) remains a popular and easily available modality for examination of ocular abnormalities<sup>[4]</sup> and is a cost effective diagnostic tool without harmful effects of ionizing radiation to the lens. 7.5-13 MHz transducers give high resolution images for visualization of the anterior and posterior segments of the eyeball. It has the added advantage of real time imaging and allows dynamic scanning synchronized with ocular movements while performing the scan. The role of USG is well established for vitreal, choroidal, and retinal abnormalities<sup>[4]</sup> and also in cases of ocular trauma. Foreign bodies (FB) within the globe, that are not radio-opaque or suspected ferromagnetic metallic FB, can be visualized easily and localized with USG. The use of Doppler has enhanced its utility in evaluation of the vessels and also helps in assessing vascularity of lesions. The main limitation of USG for orbits is its inability to image the bony architecture, lack of detailed visualization of orbital apex and for intracranial extension of various pathologies.<sup>[1]</sup>

Computed tomography (CT) and Magnetic resonance (MR) are used widely in imaging of the orbits and each has its advantages and pitfalls. The protocols for CT/(MR) should be planned as per clinical indication. Intravenous (IV) contrast in recommended doses should be used as required to evaluate enhancement.

Routine CT exams are obtained parallel to the orbitomeatal line (OML) with 3 mm contiguous axial sections, with thinner slices up to 1-2 mm, when required. Direct 2-3 mm thin coronal sections perpendicular to OML may be required. Multidetector CT (MDCT) has the advantage of rapid acquisition of volumetric dataset (isotropic imaging) allowing excellent multiplanar reconstruction (MPR) images. Non-ionic iodinated contrast (300 mg/ml) is used in

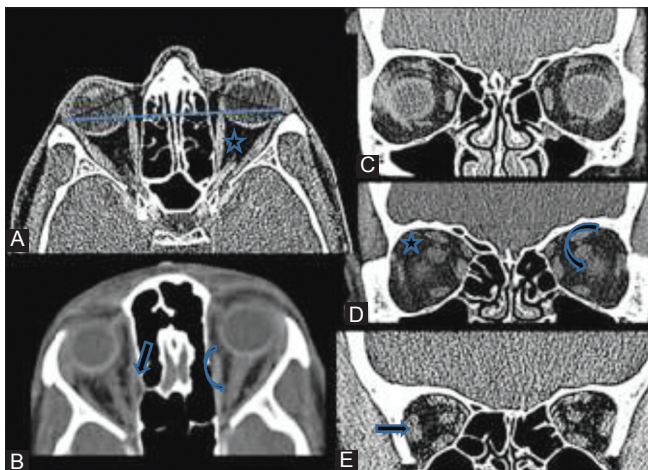


**Figure 1 (A-E):** Computed tomography sections in axial (A and B) and coronal (C-E) show normal anatomy of bony orbital walls with extraocular muscles (arrow), optic nerve (curved arrow) within hypodense orbital fat (asterisk) and long axis anterior (base) to posterior (apex) is directed lateral to medial

appropriate doses to assess the tissue enhancement patterns in many orbital conditions.

Radiation dose to the lens (at least 50 mGy or more) needs to be remembered. Proptosis can be objectively assessed on axial CT<sup>[1]</sup>. Normally, at least one third of the eyeball lies posterior to the line joining lateral orbital margins in axial scans [Figure 1A, blue line].<sup>[1]</sup> MR images obtained using head coil on a high field strength magnet (1.5-3.0 T) enables adequate visualization at orbital apex and beyond. Short scan times with turbo/fast spin echo (SE) sequences, T1W, T2W without and with fat suppression (FS) techniques like short tau inversion recovery (STIR) images. Thin (3 mm or less) slice thickness with acquisition in at least two scan planes, small field of view (FOV), high resolution matrix (256 × 256) and T2W imaging of the brain for evaluation of the entire visual pathways. Gadolinium (Gd) enhancement is seen as high intensity in post-contrast FS T1W images. Additional sequences with Gradient echo images (GRE) can be acquired depending on the indication.

### Inflammatory diseases

#### Infections/cellulitis

Bacterial infections are amongst the commonest pathologies constituting nearly 60% of primary orbital pathologies,<sup>[1,5]</sup> majority of which originate from the paranasal sinuses. It is the most common cause of proptosis in children.<sup>[6]</sup> CT and MRI can demonstrate the various stages of orbital cellulitis<sup>[7]</sup> [Figure 3A and B]: Edema, (not a stage of orbital cellulitis) phlegmon and abscess formation [Figure 4]. Complications like cavernous sinus thromboses and intracranial extension<sup>[7]</sup> can be detected early.

Orbital fungal infections like mucormycosis or aspergillosis may follow an aggressive course in patients with diabetes

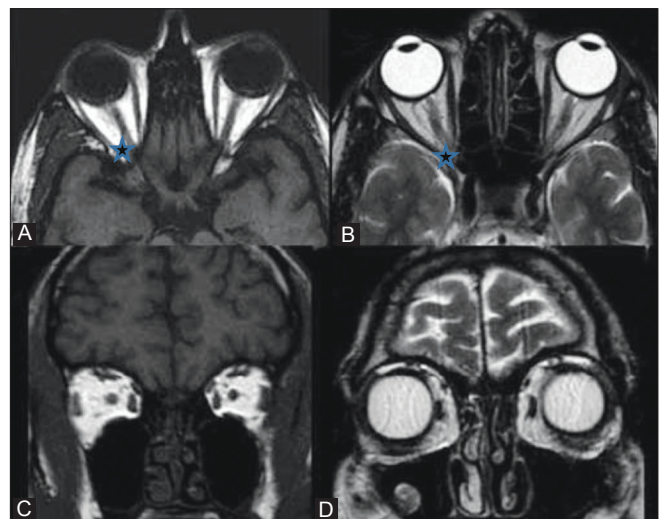


**Figure 2 (A-D):** Magnetic resonance images show normal intraorbital and intraocular contents (globe) in axial and coronal T1WI (A), (C) with better anatomic detail, T2WI (B) T2WI (D) with more contrast resolution for the soft tissues. Apex is very well visualized (asterisk)

mellitus or an immunocompromised status<sup>[1]</sup> sometimes resulting in intracranial extension [Figure 5].

*Idiopathic non-granulomatous inflammatory syndrome:*

Patients with Inflammatory orbital syndrome (IOS) (also called as orbital pseudotumour) present with acute or sub acute pain<sup>[1]</sup> and swelling associated with restricted eye movements and may sometimes be bilateral.<sup>[8]</sup> There is usually no local or systemic cause found.<sup>[8,9]</sup> The common types of IOS are:

- Anterior orbital group which is characterized by uveal-scleral thickening and inflammation at optic nerve junction with enhancement on CT/MR. It needs to be differentiated from orbital cellulitis or leukemic infiltration.<sup>[9]</sup>
- Diffuse type represents a -tumefactive or infiltrative process, involving retrobulbar space without bony

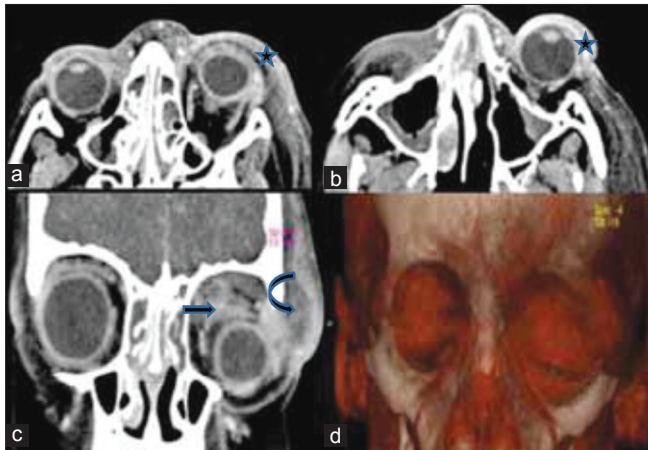


**Figure 3A:** Orbital cellulitis, left. Axial post-contrast computed tomography sections (a and b) show eyelid edema (asterisk), enhancing thickened sclera, extraocular muscles (arrow) with sinusitis causing proptosis. Coronal (c), volume rendered (d) images shows boggy collection (phlegmon) [curved arrow] with displacement of the globe

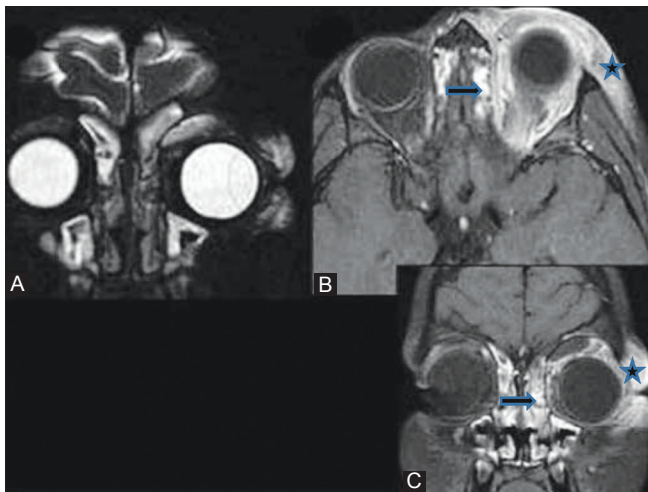


**Figure 4 (A-C):** T2W coronal magnetic resonance images (A), post-contrast T1W FS axial, coronal images (B and C) shows left orbital cellulitis with subperiosteal abscess (asterisk) with bilateral pansinusitis (arrow)

erosion. A differential diagnosis of lymphoma should be considered.<sup>[9]</sup>

- Myositic type of IOS is an inflammation of the extra ocular muscles. CT/MRI show enlarged muscles with shaggy margins, typically involving the tendons up to the insertion with enhancement and obliteration of peripheral surgical fat planes, usually affecting the superior group [Figure 6] and medial rectus and should be differentiated from thyroid myopathy.<sup>[9]</sup>
- Lacrimal gland inflammation<sup>[1]</sup> has a similar imaging appearance as sarcoid or lymphoma of the lacrimal gland.
- Orbital apex inflammation<sup>[1]</sup> infiltrating posteriorly into optic nerve sheath complex (ONSC) or posterior EOM involvement.
- Tolosa-Hunt syndrome<sup>[1]</sup>, which is characterized by painful external ophthalmoplegia [Figure 7].

*Parasitic infestations*

Parasitic infestations are common in the tropical countries and may be related to certain occupations

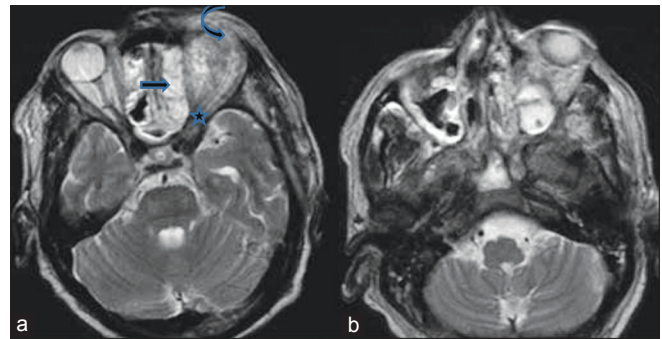


**Figure 3B:** Magnetic resonance T2W axial images (a and b) show left orbital cellulitis diffusely involving preseptal and postseptal tissues with myositis (curved arrow) extending upto the orbital apex (asterisk) and associated sinusitis (arrow)

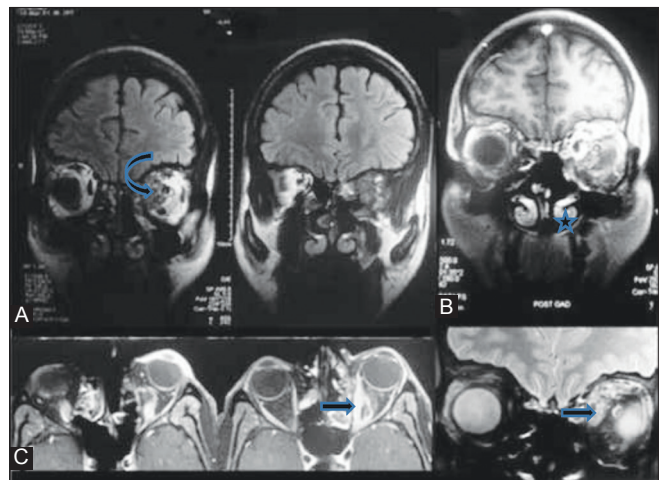


**Figure 5 (A-C):** Mucormycosis in human immunodeficiency virus (HIV) positive patient with left proptosis. Coronal T1WI (A) show hypointense areas (curved arrow) within medial aspect of hyperintense orbital fat. Signal void within ethmoid air cells (apparent aerated sinus) is misleading. Post-contrast T1WI FS (B and C) show enhancement of medial rectus (arrow) and enhancing sinonasal mucosa (asterisk) suggesting inflammation

and environmental conditions. They are endemic in regions with poor hygiene and sanitation as human infestation occurs due to ingestion of ova in food or water. Larval forms may be found as cysts within orbital tissues which may be detected by imaging, [Figure 8] Cysticercosis may involve EOM and can be associated with neurocysticercosis [Figure 9]. The differentials on imaging are other granulomatous orbital lesions [Figure 10] e.g., tuberculomas. Toxocara infestation may cause inflammation (endophthalmitis) when they die, which can present with leucocoria in children.

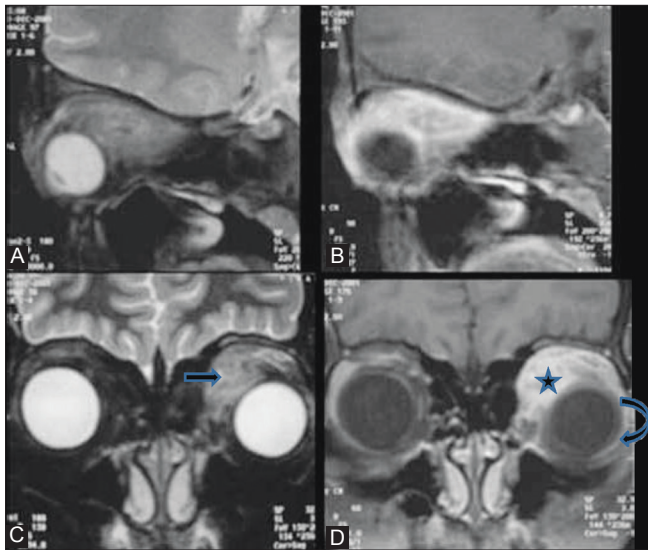


**Figure 6 (A-D):** Orbital pseudotumor. Axial and coronal T2W (A and C) images show minimal hyperintensity of globe with uveo-scleral thickening (curved arrow) (Tenon's fasciitis), inflammation (arrow) of muscle and surrounding orbital fat with enhancement (asterisk) in post-contrast T1WI FS (B and D)

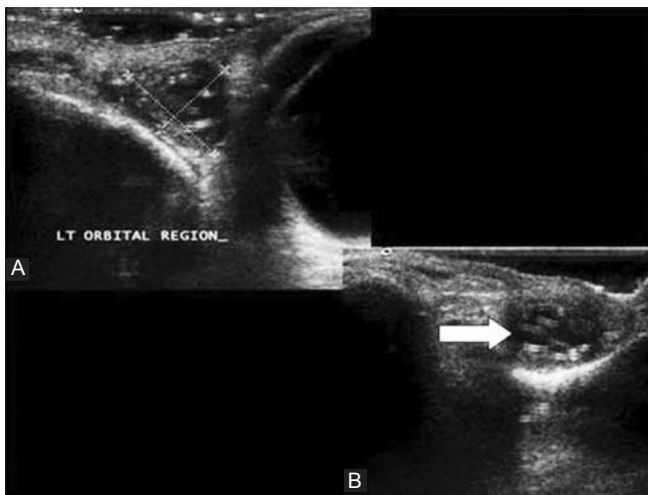


**Figure 8 (A, B):** (A, B) Swelling medial aspect of left orbit. High resolution USG left orbit shows linear, serpiginous contents within extraocular cystic lesion (arrow) with distal enhancement medial to globe. Realtime slow movements of these structures were seen during scanning. Live adult filarial worms were seen on surgery

**Graves' dysthyroid ophthalmopathy/graves' orbitopathy (GO)**

Graves ophthalmopathy is one of the commonest causes of exophthalmos in adults and is almost always bilateral although asymmetric involvement may be seen in few. It is presumed to be an autoimmune condition with a female preponderance consisting of a triad of goiter with hyperthyroidism, infiltrative ophthalmopathy, and dermatopathy. CT/MRI can be used to assess and follow-up the changes in response to steroid and/or immunomodulatory therapy. EOM are enlarged with sparing of tendons. The muscle margins are sharply defined with preserved fat planes. There is increased volume of retro-orbital fat with bulging of orbital septum anteriorly [Figure 11]. Involvement of the inferior rectus precedes involvement of the superior and the medial rectus.<sup>[9]</sup> In cases with isolated lateral rectus involvement, other differentials need to be considered. CT may show low density within the muscles due to deposition of lymphocytes and mucopolysaccharides. MRI reveals T2 hyper intensity due to infiltration and interstitial edema of involved EOM in active disease which can be easily demonstrated in T2W inversion recovery sequences (TIRM) with FS.<sup>[10]</sup> The cross-sectional area of the most inflamed EOM muscle belly can be measured on 3 mm coronal T2W IR fat suppressed sequences<sup>[10]</sup> EOM enlargement can be easily measured as its maximum radial diameter of the belly of the involved muscle in coronal sections.<sup>[11]</sup> This can be used for objective follow-up to assess response to therapy

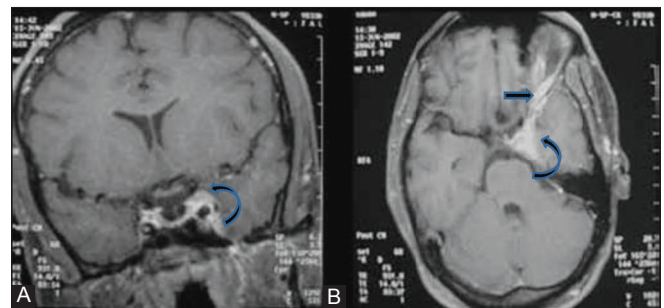


**Figure 7 (A, B):** Tolosa-Hunt syndrome subtype. T1W FS post-contrast gadolinium coronal (A), axial (B) shows enhancing inflammatory infiltration in the left orbital apex (arrow) extending into the cavernous sinus (curved arrow)

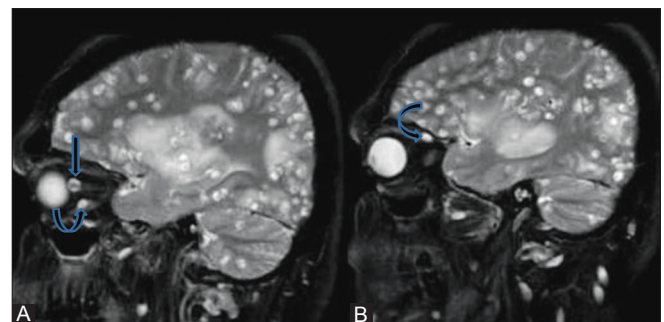


**Figure 9 (A, B):** Cysticercosis. Magnetic resonance T2W sagittal sections show multiple hyperintense cysticerci with hypointense eccentric scolices in the orbit within (A) optic nerve (arrow) and inferior rectus muscle (curved arrow) and (B) superior rectus muscle (curved arrow). Note heavy infestation of brain and other soft tissues

with steroids. In chronic disease, atrophy of EOM may be seen with fat replacement which can be detected on T1W images without FS.

There may be associated compressive optic neuropathy probably as a result of pressure at the orbital apex by increased volume of orbital contents, overcrowding and stretching of the nerve due to proptosis.<sup>[10]</sup> High-resolution volume acquisition (T1W-3D) with curved multiplanar reformatting can be used to measure the optic nerve diameter along its entire length.<sup>[11]</sup> Decompression surgery may prevent irreversible optic nerve atrophy in early stage of disease.

**Orbital trauma**

CT is the modality of choice in evaluation of

orbital trauma.<sup>[1]</sup> Bony fractures and displacements, small comminuted fragments [Figure 12], and radio-opaque foreign body (FB) are best seen on CT. Volume rendering techniques (VRT) with MDCT allow excellent 3D reconstructions that help surgeons to visualize the fractures in relation to other anatomic structures and evaluate treatment plans<sup>[12]</sup> [Figure 13]. Blowout fractures classically involve the floor with sparing of the orbital rim. The orbital contents including the orbital fat, inferior rectus and the inferior oblique muscles may herniated through the floor of the orbit into the maxillary antrum due to increased intra orbital pressure.<sup>[1]</sup> [Figure 14A]. Soft tissue injury, inflammation, muscle herniation, and entrapment [Figure 14B] are well visualized with CT/MRI

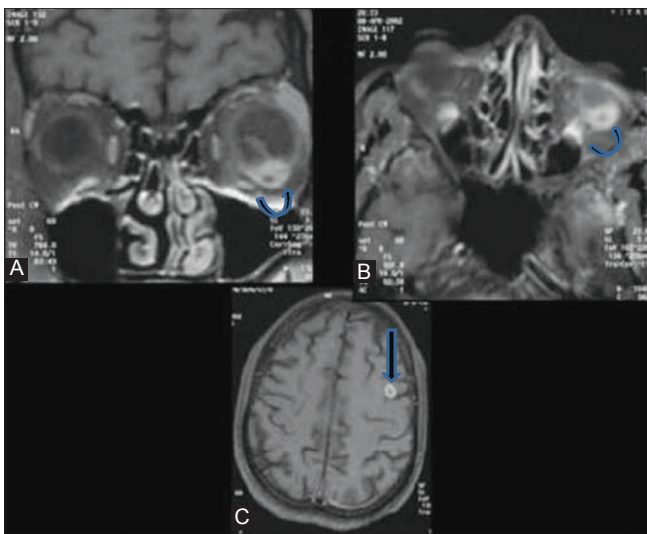


**Figure 10 (A-C):** Coronal (A), axial (B) post-contrast gadolinium-enhanced T1W FS images shows enhancing intraocular lesion (curved arrow) in left orbit and axial T1WI of brain (C) reveals intracerebral ring enhancing lesion (arrow) in left parietal lobe suggestive of typical granulomatous lesions

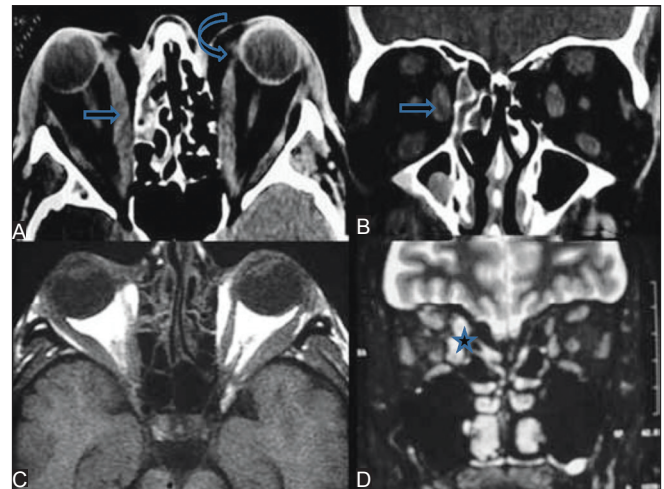


**Figure 11 (A-D):** Bilateral exophthalmos in thyroid orbitopathy. Axial (A), coronal (B) computed tomography sections show bilateral enlargement of extraocular muscles, prominent involving medial rectus (arrows) with sparing of tendons (curved arrow). Axial T1W (C) Magnetic resonance images shows enlarged bulky extraocular muscles (asterisk), mildly hyperintense on coronal T2W (D)

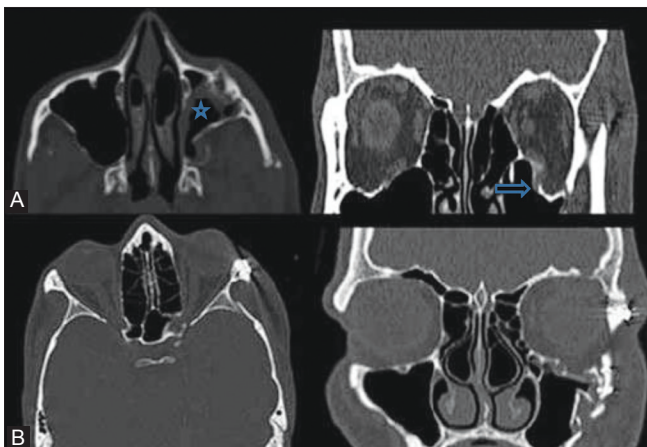


**Figure 12 (A, B):** (A, B) Facial trauma with multiple fractures. Computed tomography sections in bone windows show comminuted fractures involving facial bones on left with multiple displaced bony fragments, depressed orbital floor (arrow) and collapsed ipsilateral maxillary antrum (asterisk)

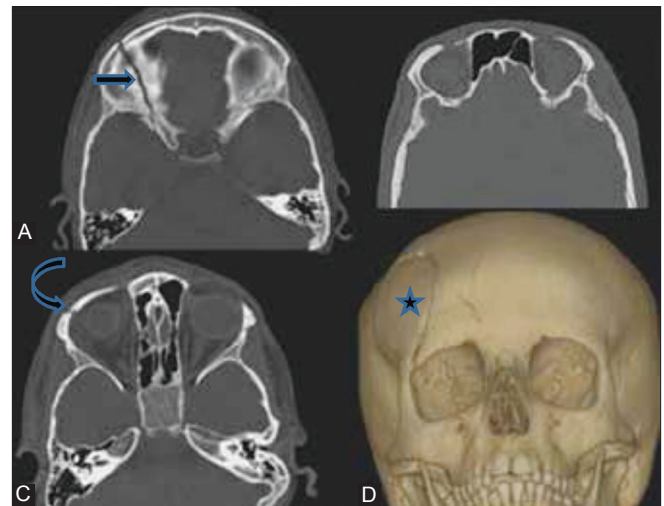


**Figure 13 (A-D):** Orbital Trauma. Axial computed tomography with bone window displays right sided fracture of orbital roof (arrow) (A), superior orbital rim (curved arrow) (B, C) which are very well seen images with volume rendering techniques (asterisk) (D)

on axial and coronal sections. Associated vascular and nerve injury, and intracranial hematomas<sup>[1]</sup> are better evaluated with MRI [Figure 15]. However, MR is contraindicated if there is suspicion of intraocular ferromagnetic FB.

**Tumors**

The orbit may be involved by tumors which are primary masses arising from the various orbital structures.

*Lymphoid neoplasms*

These range from the benign reactive lymphoid hyperplasia to malignant lymphomas and are more commonly seen in adults and very rarely in children.<sup>[6]</sup> All such patients should undergo evaluation to rule out a systemic lymphoproliferative disorder.<sup>[1]</sup> Malignant lymphoma, either arise in and are limited to the orbit or extend into the orbit arising from the sino-nasal cavities.<sup>[6]</sup> Imaging is not specific in differentiating them from pseudotumors. CT and MR reveal enhancing, solid soft tissue masses in the retrobulbar region [Figure 16] without bony

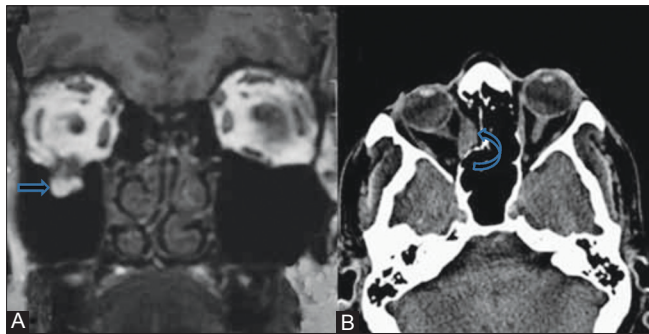


**Figure 14 (A, B):** T1W coronal image (A) shows classic blowout fracture of floor of right orbit with herniated contents into the roof of maxillary antrum (arrow). Axial computed tomography (B) shows herniation of medial rectus into adjacent ethmoid sinus (curved arrow) with fracture of right lamina papyracea

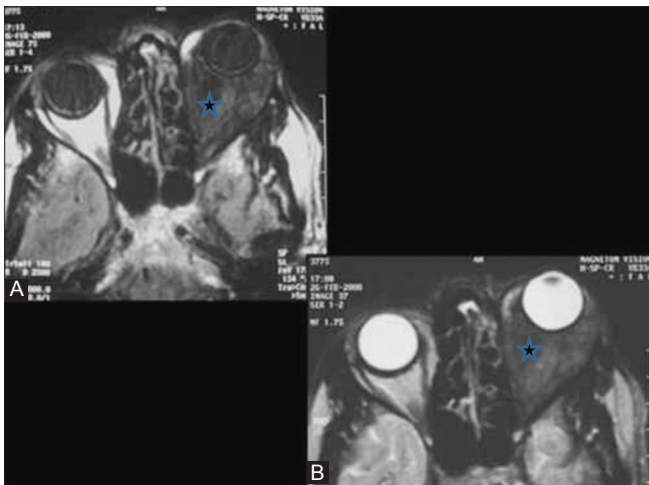


**Figure 16 (A, B):** Lymphoma left orbit in a case of unilateral proptosis. Axial magnetic resonance shows diffusely infiltrating lesion involving left retrobulbar region (asterisk), appearing hypointense to orbital fat on T1WI (A), hypointense on T2WI (B) with preseptal soft tissue thickening

destruction, except rarely in very aggressive malignant variants.<sup>[13]</sup> Lacrimal gland lymphoma shows enhancement and enlargement with associated displacement of the globe medially.<sup>[14]</sup> MR is more sensitive in visualizing early infiltration of ocular structures.

*Leukemias*

Orbital involvement is due to infiltration of soft tissue or orbital bone, usually in Acute lymphoblastic leukemia (ALL) (up to 75%)<sup>[15]</sup> and 20% in Acute myeloid leukemia (AML) (Chloromas).<sup>[15]</sup> CT/MRI may reveal a sub-periosteal lesion [Figure 17] involving the lateral wall of the orbit, which may extend into the temporal fossa or a mass on the medial wall involving ethmoid sinuses extending through the cribriform plate into the anterior cranial fossa.<sup>[1]</sup> Meningeal infiltration and intracranial extension can be detected early in post-contrast scans. Vascular lesions represent a large group of vascular malformations involving the orbit.<sup>[16]</sup> MRI has the advantage over CT as it is very sensitive in detecting blood and blood products and vessels with flow.

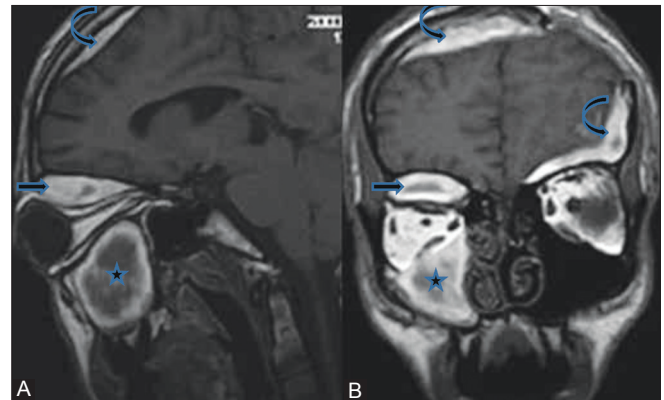


**Figure 15 (A, B):** Subperiosteal hematoma in orbital trauma. Axial (A), coronal (B) T1WI shows subacute hyperintense hematoma right orbit with mass effect (arrow). Associated hemosinus within right maxillary sinus (asterisk) and subdural hematoma (curved arrow)

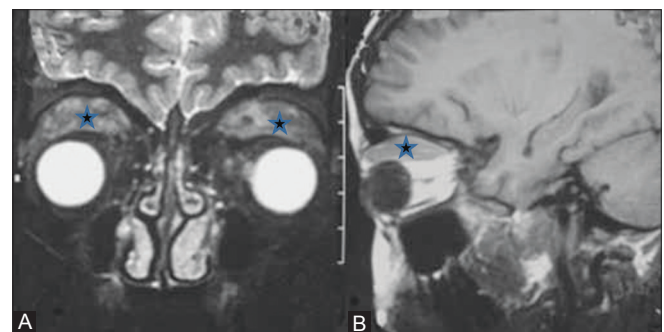


**Figure 17 (A, B):** Orbital leukemic deposits in patient with ALL. Axial Magnetic resonance short tau inversion recovery (A) shows bilateral subperiosteal lesions (asterisk) extending superior and laterally up to the lacrimal glands, hypointense to orbital fat extending posteriorly on sagittal T1WI (B)

*Cavernous hemangioma (Venous angioma)* is the commonest vascular tumor in adults presenting as a well-defined progressively increasing mass. It is usually seen on CT as a smoothly marginated, rounded enhancing soft tissue density intraconal mass that may have calcification [Figure 18]. MR T1W shows a hypointense mass, hyperintense on T2W with variable contrast enhancement [Figure 19]. Differentials of other intraconal masses like meningiomas, schwannomas or hemangiopericytoma need to be considered.<sup>[11,16]</sup>

*Capillary hemangiomas* present in infants within first year of life and then tend to diminish in size from the time of presentation due to gradual involution. They usually have definite arterial supply from either external/internal carotid artery,<sup>[16]</sup> and are composed of thin small vascular spaces due to capillary proliferation with no distinct capsule. CT/MR may show extra conal masses along the superior aspect of the orbit that may extend intracranially. These masses show intense enhancement in the early phase with early washout of the contrast in delayed phases.<sup>[1]</sup> On MR, they are usually hypointense on T1W images and have a heterogeneous appearance on T2 weighted images with evidence of flow voids within the lesion [Figure 20].

*Other vascular lesions* include lymphangioma [Figure 21], veno-lymphatic, and arteriovenous malformations.<sup>[1,16]</sup> Orbital varix present usually with intermittent proptosis and is a common cause of spontaneous orbital hemorrhage.<sup>[17]</sup>

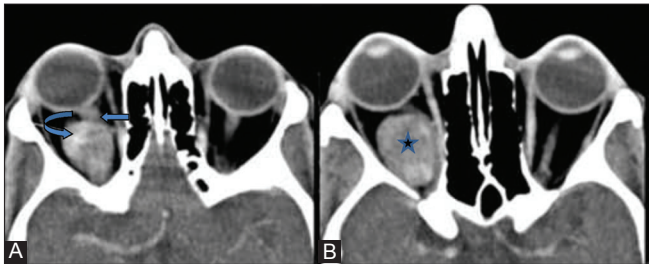


**Figure 18 (A, B):** (A, B) Cavernous hemangioma right. Axial Computed tomography shows an enhancing, smoothly marginated, rounded soft tissue density intraconal mass (asterisk) causing medial displacement of optic nerve (arrow) in a young female. Punctate focus of hyperdense calcification (curved arrow) seen within

Imaging performed in prone position can demonstrate a dilated venous channel which is usually hyperintense on both T1W and T2WI. Carotid-cavernous fistula causes pulsating exophthalmos, with engorgement of superior ophthalmic vein (SOV) which can be very well visualized on CT and MRI [Figure 22]. However, in the late stages there can be stenosis due to thrombosis of the SOV.

#### Optic nerve sheath complex

MR is the modality of choice for imaging of the entire visual pathway from its origin at the posterior point of the globe to the visual cortex.<sup>[1]</sup> Intraorbital optic nerve (ON) is seen well on CT due to the attenuation differences with surrounding hypodense retrobulbar fat. Intraorbital part of ON is hypointense on T1WI within hyperintense fat, isointense on T2WI with surrounding subarachnoid cerebrospinal fluid (CSF) within the meningeal sheath

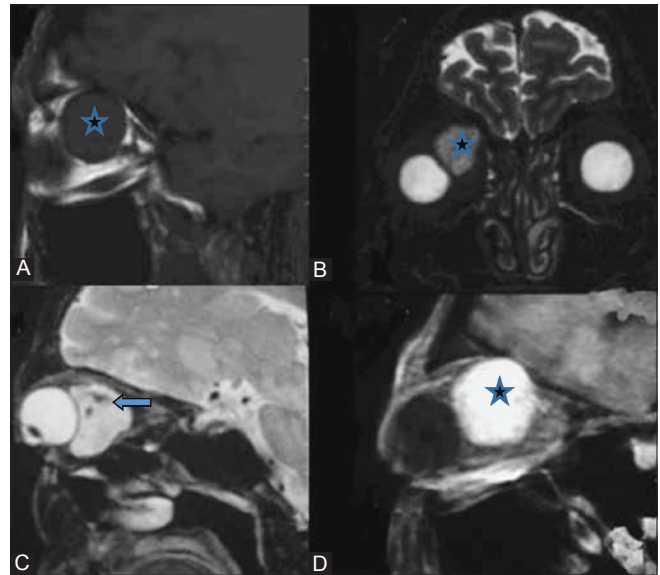


**Figure 19 (A-D):** Cavernous hemangioma-right orbit. Magnetic resonance imaging shows intraconal hypointense, rounded well-circumscribed mass lesion (asterisk) on sagittal T1WI (A), hyperintense on short tau inversion recovery (B), T2WI (C) with few hypointensities of flow voids (arrow) with intense enhancement on post-contrast gadolinium enhanced T1W FS images (D)

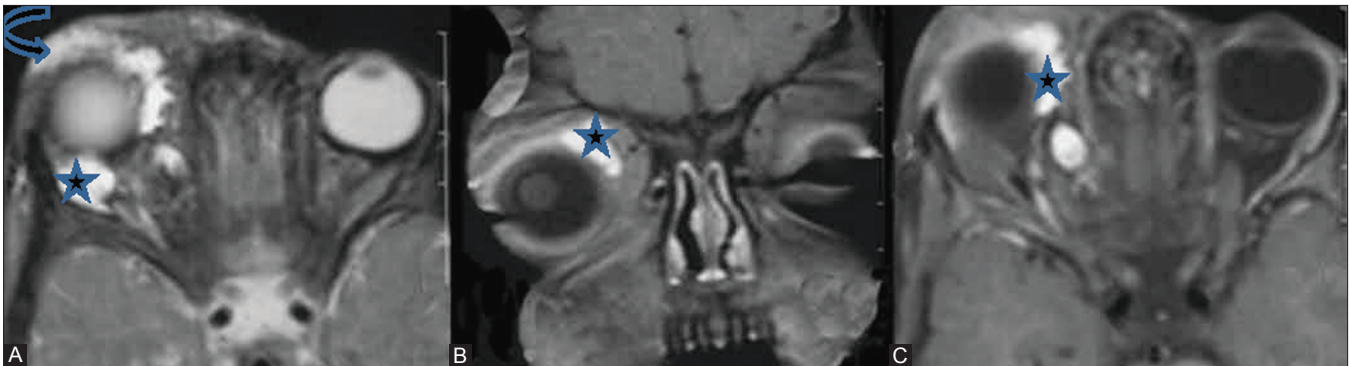


**Figure 20 (A-C):** Capillary hemangioma. Axial T2WI (A) demonstrates an irregular hyperintense lesion (asterisk) involving right orbit extending into anterior periocular tissues (curved arrow) enhancing well on contrast gadolinium administration seen on T1WI coronal (B), axial (C) images

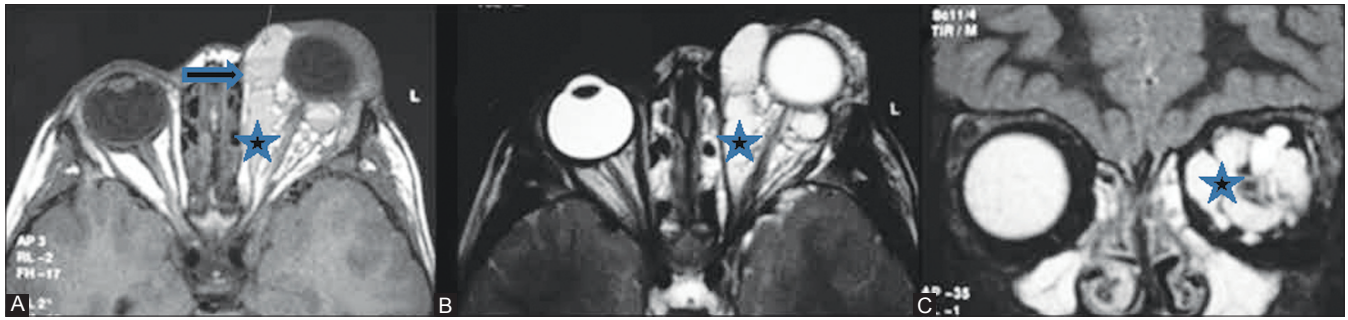


**Figure 21 (A-C):** Lymphangioma. Multiseptate, multilobulated lesion left orbit (asterisk), with multiple fluid-fluid levels within multiple locules (arrow) appears hypointense to orbital fat, hyperintense to brain on axial T1W (A), markedly hyperintense on axial T2WI (B) and coronal short tau inversion recovery images (C)

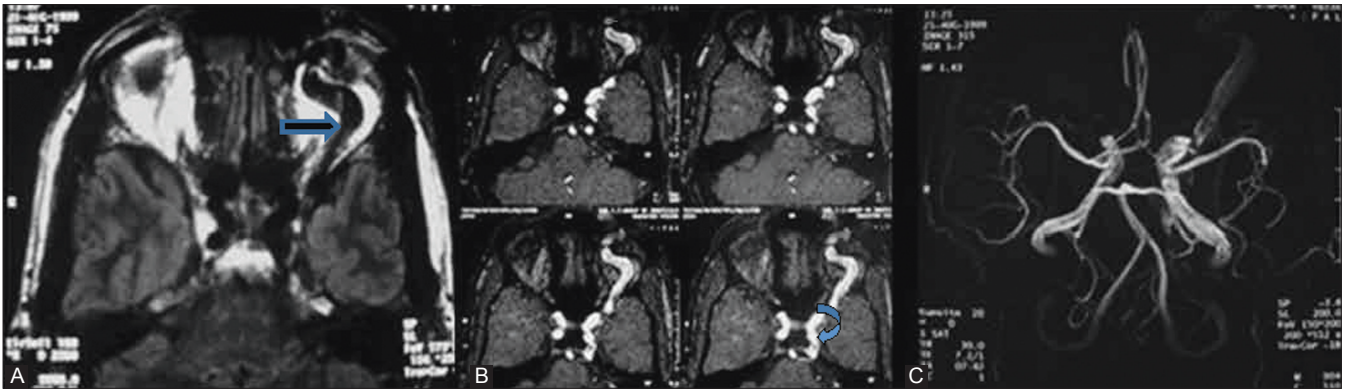


**Figure 22 (A-C):** Carotid cavernous fistula left. Axial T1WI (A) shows enlargement of superior ophthalmic vein with prominent signal void on left (arrow), distended cavernous sinus (curved arrow) on 3D TOF Magnetic resonance angiogram (MRA) (B and C)

is hyperintense. The intracanalicular portion is not well visualized on CT due to the dense cortical bone at the apex<sup>[1]</sup> and is displayed very well on MR. The intracranial ON, optic chiasma, and tracts are well visualized on coronal and sagittal MR<sup>[18]</sup> and appear isointense to cerebral white matter. The optic radiation is within the white matter of temporoparietal and occipital lobes extending upto the calcarine cortex (primary visual cortex) flanked by the easily identified calcarine sulcus on the medial aspect of the occipital lobe.<sup>[1,18]</sup>

Enlargement of ONSC can be due to primary or secondary tumors involving the ON or due to inflammatory/infiltrative processes.

#### *Optic nerve glioma*

Intraorbital gliomas appear early within first decade of life, presenting with painless proptosis, usually with associated loss of vision.<sup>[19]</sup> CT/MR shows marked fusiform enlargement of ON with kinking or buckling. Calcification is usually absent. Bilateral lesions are seen in Neurofibromatosis (NF) Type 1,<sup>[20]</sup> thus entire visual pathway should be evaluated. MR is more sensitive and 3mm thin sections are recommended which can avoid missing small lesions in the intracanalicular portion. Usually, it appears hypointense to orbital fat on T1WI (isointense to cerebral cortex), it is hyperintense to cortex, white matter and fat on



**Figure 23 (A-C):** Optic nerve glioma. T2WI sagittal (A) shows fusiform enlargement optic nerve (asterisk) with hyperintense perineural meningeal circumferential thickening (arrow) on short tau inversion recovery coronal T2WI (B) (arachnoid gliomatosis) in optic nerve glioma and significant enhancement (curved arrow) on T1W FS image (C)

T2WI. Post-contrast enhancement is common except in areas with cystic changes,<sup>[19-21]</sup> [Figure 23]. Sometimes, the tumor grows circumferential around the ON into the perineural space to mimic a peri-optic meningioma<sup>[1]</sup> [Figure 24].

#### *Optic nerve sheath meningioma*

These are usually benign tumours arising from the meningo endothelial cells with a higher incidence in females They commonly occur in the 4<sup>th</sup>-5<sup>th</sup> decade, however if they are found in children, a possibility of Neurofibromatosis type II needs to be kept in mind. The patterns usually seen on imaging are as an eccentric localized mass on one side of the optic nerve or circumferential along the length as thickening or fusiform enlargement of the ONSC.<sup>[19]</sup>



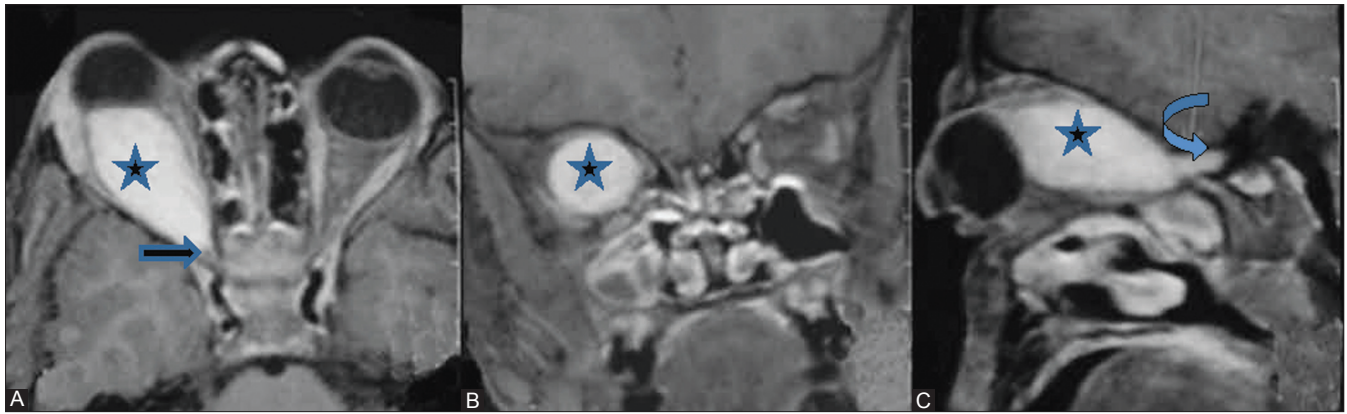


**Figure 24 (A-C):** Post-contrast T1W FS axial (A), coronal (B), Sagittal (C) showing smooth fusiform expansion of optic nerve sheath complex (asterisk) with diffuse homogeneous enhancement extending posteriorly through the apex (arrow) along the visual pathway (curved arrow) suggestive of optic nerve glioma

Intratumoral calcification is common and is well detected on CT. It may cause bony hyperostosis and optic canal enlargement<sup>[19,20]</sup> [Figure 25]. It shows decreased signal intensity on both T1W and T2W MRI. Post-contrast enhancement is marked [Figure 26] and “tramtrack” type in circumferential type of lesions,<sup>[1]</sup> Diagnosing intracanalicular meningiomas is a challenge<sup>[22]</sup> and Gd-enhanced MRI with FS helps in detection of tiny lesions, especially at the orbital apex.<sup>[23]</sup> In children, they tend to be more aggressive and may infiltrate into other orbital structures.

*Optic neuritis*

Acute inflammation causes enlargement of ON due to infections by micro-organisms causing papillitis, or following viral infections due to immune mechanisms (parainfections).<sup>[1]</sup> Non-infective granulomatous diseases like sarcoidosis, systemic autoimmune diseases like systemic lupus erythematosus (SLE) may involve the ON.<sup>[24]</sup> Optic neuritis is an early manifestation of multiple sclerosis (MS) which is seen well on MRI as thickening with focal hyperintense plaques on T2WI and better seen on STIR images<sup>[25]</sup> [Figure 27]. FS T1WI pre- and post-contrast images are useful in optic neuritis and demonstrates localized or diffuse enhancement within the nerve [Figure 28]. Brain and spine MRI is usually required in combination while evaluating patients of demyelinating diseases such as MS.

The orbit may be secondarily involved due to invasion of malignant tumors from the surrounding structures, most commonly malignancy from sino-nasal cavities [Figure 29] or due to metastatic deposits from known or unknown primary.<sup>[1]</sup> The most common primary cancers in adults are breast, prostate gland, and lung cancer. In about 10% of patients who present with ophthalmic symptoms due to secondary deposits, the primary site remains obscure in spite of detailed systemic evaluation. In the pediatric age group, neuroblastoma is one of the commonest primary tumors that metastasise to the orbits.

Diffusion weighted imaging (DWI) MRI with apparent

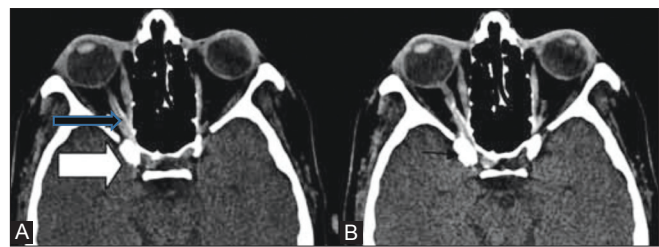


**Figure 25 (A, B):** Peri optic meningioma. Thin sections axial computed tomography shows (A) tramtrack calcification along right optic nerve sheath complex (thin arrow), hyperostosis at optic canal (thick arrow). Post-contrast perineural enhancement noted (B)

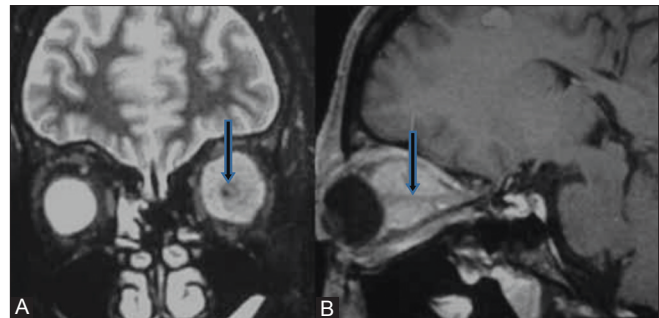


**Figure 26 (A, B):** Optic nerve sheath complex meningioma. Magnetic resonance short tau inversion recovery coronal (A), sagittal post-contrast fat suppression T1WI (B), left intraconal mass with fusiform thickening of perineural portion of optic nerve sheath complex compressing the nerve (arrow) splaying of muscle cone showing diffuse enhancement

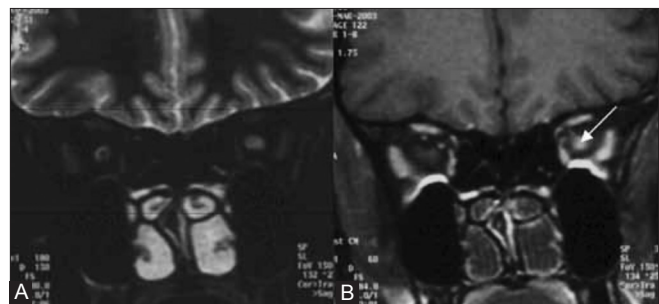


**Figure 27 (A, B):** (A, B) Optic neuritis. Magnetic resonance short tau inversion recovery coronal images show increased signal intensity of optic nerve sheath complex with slightly enlarged nerve (arrow) (Normal optic nerve measures 3-4 mm)

diffusion coefficient (ADC) values and ratios are being increasingly used to analyze molecular diffusion at the cellular level in head and neck imaging, especially in cancers.<sup>[26]</sup>

**Ocular tumors**

*Retinoblastoma*

Retinoblastoma is the commonest intraocular tumor of childhood (usually presenting below 5 years) and is thought to be congenital in origin.<sup>[1]</sup> It is a malignant tumor arising from the neuroectodermal cells of the retina and must be differentiated from other benign lesions for early management and better prognosis. Clinically, leucocoria<sup>[27]</sup> is associated with proptosis, which may be bilateral. The main patterns of the lesion are exophytic,

endophytic or diffuse type.<sup>[1]</sup> The intraocular mass with calcification and areas of necrosis, associated retinal detachments and vitreous involvement (endophytic type) can be well visualized on USG. CT and MRI are very useful in determining retrobulbar and extraocular spread, intracranial involvement, and exclude trilateral retinoblastoma with pineal gland tumors when bilateral disease is detected. CT is very sensitive as >90% of tumors show evidence of calcification<sup>[1]</sup> [Figure 30]. On MR, they are hyperintense to normal vitreous on T1WI, moderate to markedly hypointense on T2WI depending on the calcification [Figure 31], demonstrated well with contrast administration and thin sections (1.5-3 mm) with fat-suppression. It is important to differentiate the tumor from persistent hyperplastic primary vitreous (PHPV) [Figure 32], retinopathies of prematurity (ROP), Coats' disease (primary retinal telangiectases), organized subretinal hemorrhage, endophthalmitis, and other intraocular masses.<sup>[26]</sup>

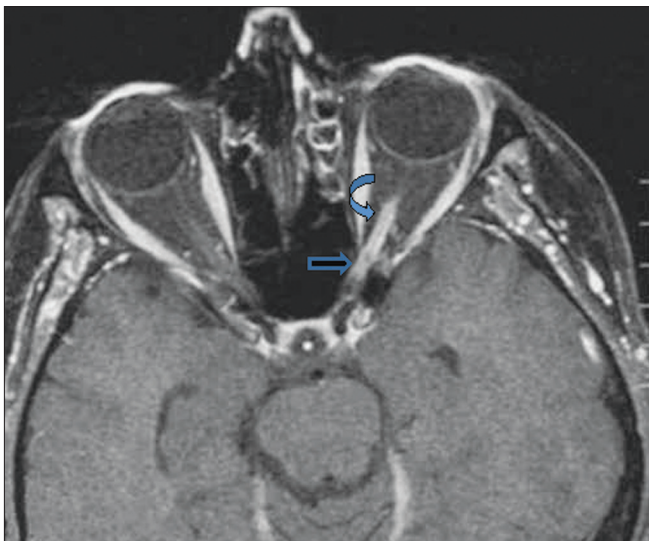


**Figure 28:** Optic Neuritis in multiple sclerosis. Axial T1WFS image showing enhancement of segment of left intraorbital (curved arrow) optic nerve extending posteriorly involving the intra-canalicular portion (arrow)

*Malignant melanoma*

These are highly malignant tumors arising from the uvea (choroid, ciliary body, iris), that tend to metastasize hematogenously to liver, lung, bone, kidney, and brain. Imaging must focus to search for metastatic spread which guides management. CT reveals a hyperdense, well-margined, typically enhancing mass and should to be differentiated from other primary and secondary uveal

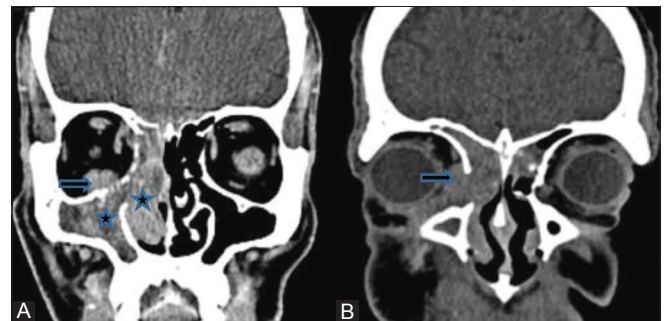


**Figure 29 (A, B):** Orbital involvement in sinonasal malignancy. Coronal computed tomography (A) shows expansile enhancing mass (asterisk) in sinonasal cavity right causing erosion of adjacent orbital bony walls (B) and extension into right orbit (arrow)

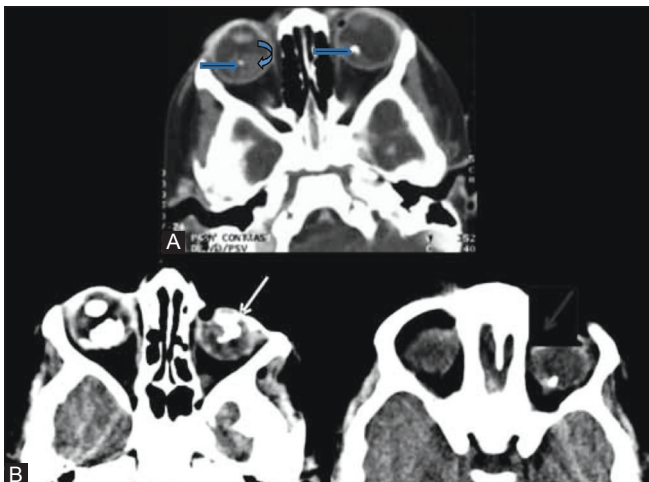


**Figure 30 (A, B):** Bilateral retinoblastomas. Axial computed tomography (CT) scans (A) showing bilateral intraocular soft tissue density mass lesions (curved arrow) with specks of calcifications (arrow). Follow-up CT (B) shows chunky calcifications with shrunken globe (ptysis bulbi) left (arrow)

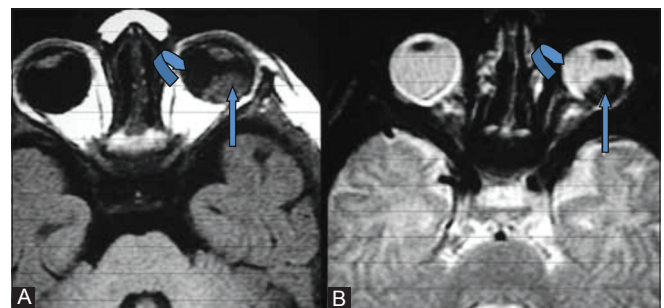


**Figure 31 (A, B):** Retinoblastoma. Magnetic resonance axial T1WI (A) shows a left intraocular mass (arrow) hyperintense to vitreous and markedly hypointense to vitreous (curved arrow) on axial T2WI (B)

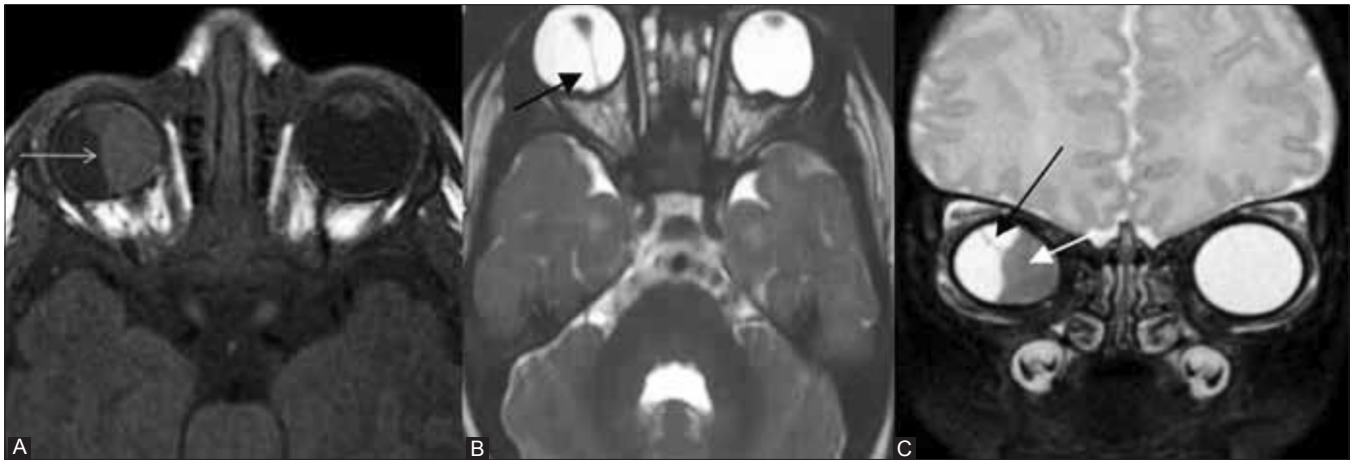


**Figure 32 (A-C):** Persistent hyperplastic primary vitreous right. Magnetic resonance T1W axial (A) shows hyperintense fluid level within hypointense vitreous (white arrow), axial (B) shows thin hypointense band (black arrow) from back of lens to posterior inner surface of globe (congenital non-attached retina/Cloquet's canal) within hyperintense vitreous, T2W coronal (C) shows fluid-fluid level

and choroidal tumors. On MR, the lesions are of moderately high signal on T1W (paramagnetic properties of melanin or hemorrhage) [Figure 33], and are hypointense on T2W. Gd contrast is used for evaluation of ON and retrobulbar extension.<sup>[27]</sup>

#### Lacrimal gland and fossa lesions

Lacrimal gland is located in the lacrimal fossa in the superolateral, extraconal compartment adjacent to superior and lateral rectus tendons]. Inflammatory diseases are usually acute, may be a part of spectrum of orbital pseudotumor or related to trauma.<sup>[28]</sup> Chronic dacryoadenitis may be associated with connective tissue disorders, non-infective granulomatous diseases (Sarcoidosis, Wegener's), Mikulicz syndrome or other non-specific infiltrative conditions.<sup>[1]</sup> CT/MR demonstrates unilateral or bilateral diffuse enlargement of the gland with marked contrast enhancement [Figure 34], and associated adjacent Superior rectus / Lateral rectus myositis or tendinitis.

Lymphomatous processes may be unilateral or bilateral, ranging from benign infiltration to malignant lymphomas, often causing diffuse enlargement. Tumors of epithelial origin represent half the masses involving the lacrimal gland; 50% of these are benign pleomorphic adenomas.<sup>[28,29]</sup> Bony changes in the fossa may be seen on CT/MRI associated with indentation of the globe and distortion of the muscle cone [Figure 35A and B].

#### Miscellaneous conditions

Post-transplantation lymphoproliferative disorder (PTLD) Seen in 2-3% patients, within first year after organ transplantation, due to uncontrolled lymphocytic proliferation response.<sup>[30]</sup> Orbit is a common site for this lesion, seen as soft tissue mass in lacrimal region, may have contrast enhancement, and at times aggressive as opposed to lymphoma [Figure 36A and B].

Craniofacial abnormalities and craniosynostosis affects

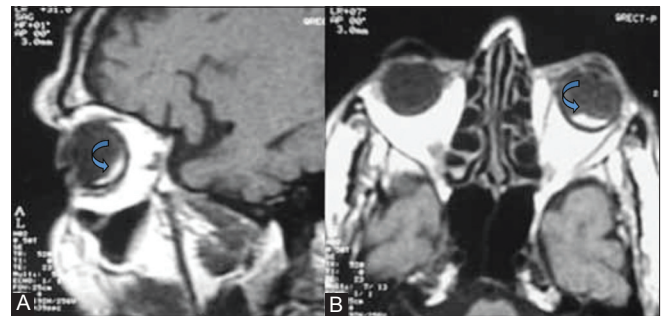


**Figure 33 (A, B):** Ocular melanoma. T1WI sagittal (A), axial (B) shows hyperintense ring shaped posterior intraocular uveal lesion (curved arrow)(paramagnetic effect of melanin)

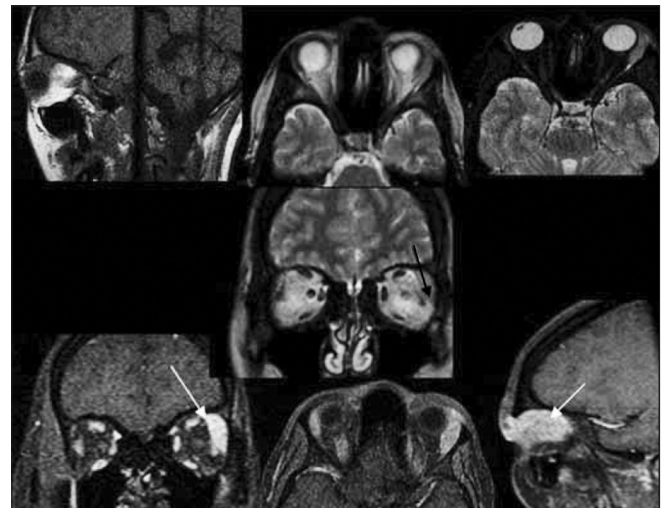


**Figure 34:** MR T1W, T2W coronal, axial images shows hypointense enlarged left lacrimal gland enlargement (black arrow) with prominent enhancement (white arrows) seen on post-contrast gadolinium enhanced T1W FS images suggestive of dacryoadenitis, mimics inflammatory pseudotumor

the development of the calvarium and facial bones which usually result in secondary changes of cranial fossae, skull base, and cranial vault and orbits. There may be other congenital developmental abnormalities associated.

Tumor-like conditions of the craniofacial bones like *Fibrous dysplasia (FD)*<sup>[31]</sup> with extensive involvement of the maxilla, mandible, and skull base may lead to anatomic deformities of the orbit and encroachment of the neurovascular canals<sup>[1]</sup> [Figure 37]. CT is the gold standard for imaging and 3D reformats are very useful in pre-operative assessment and post-surgical follow-up.<sup>[32]</sup> MR is the preferred modality for imaging of associated brain and spinal abnormalities in the evaluation of various craniofacial syndromes.

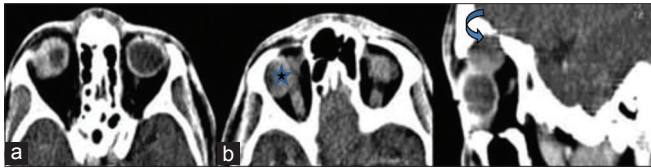


**Figure 35A:** Contrast enhanced CT images (CECT) show enhancing mass lesion of the right lacrimal gland (asterisk) with mass effect (a) and remodeling of adjacent bone (curved arrow) (b)

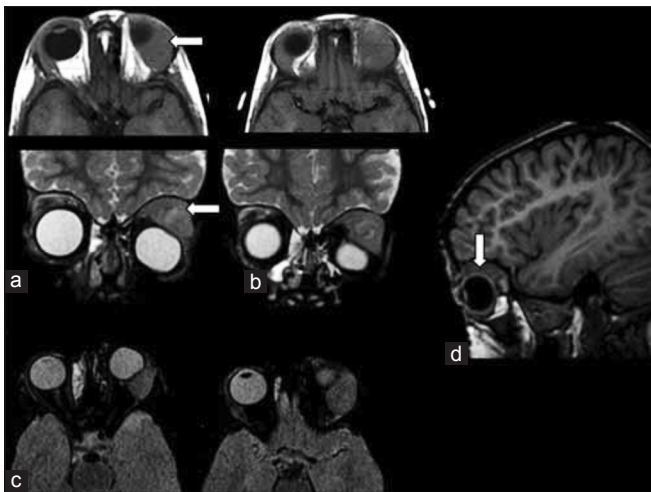


**Figure 36A:** Post-bone marrow transplant in a patient of acute leukemia with left proptosis. Magnetic resonance T1WI axial (a), sagittal (d) shows extraconal space infiltration on left (small on right), hypointense to orbital fat (white arrow), short tau inversion recovery coronal (b), axial (c) shows hypointense lesions involving lacrimal glands extending superiorly and displacing the left globe

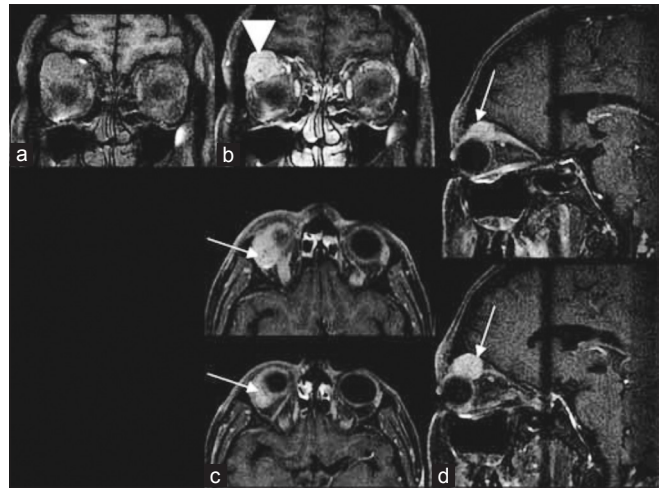


**Figure 35B:** Lacrimal gland pleomorphic adenoma. Magnetic resonance T1W FS image (a) shows enlarged globular right lacrimal gland (white arrow head), hypointense with enhancement in post-contrast gadolinium enhanced images (b-d) (white arrows) suggestive of benign tumor

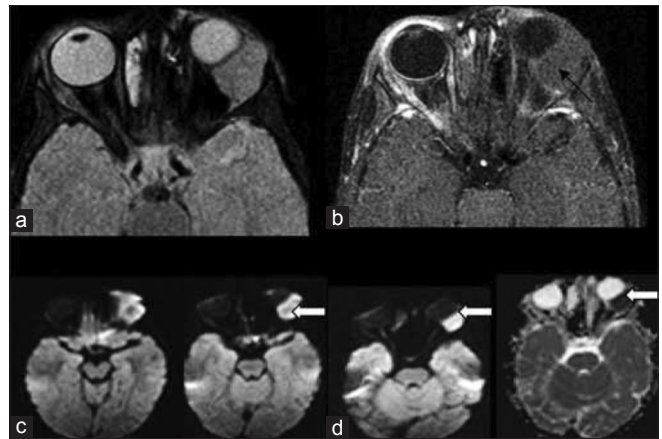


**Figure 36B:** Lesion on magnetic resonance axial short tau inversion recovery (a), post-contrast T1W FS (b) shows no enhancement (black arrow), with true restriction of diffusion appearing bright on diffusion weighted imaging axial (c) with increasing B values (0,500,1000) and correspondingly dark on apparent diffusion coefficient map (white arrows)

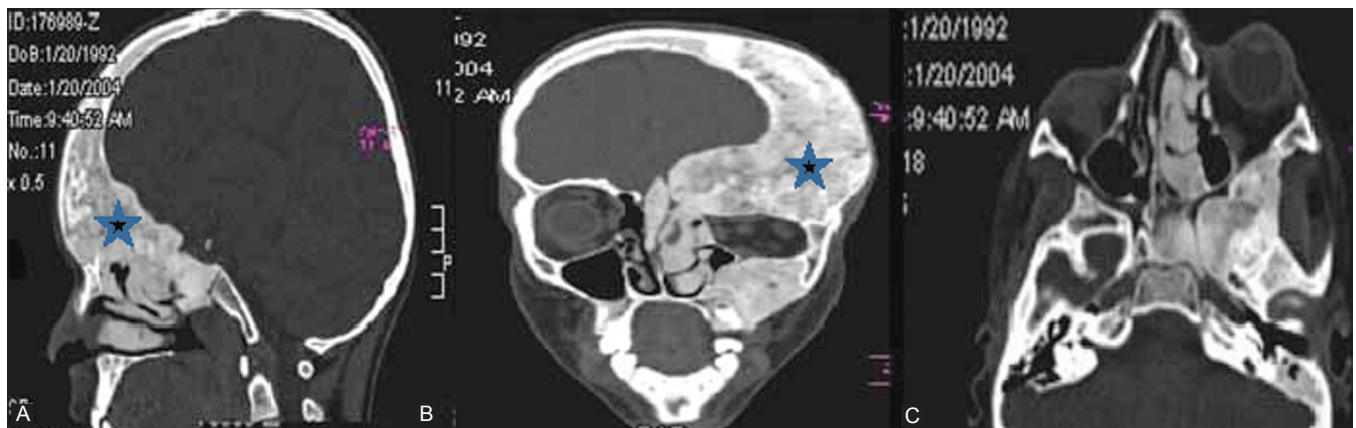


**Figure 37 (A-C):** (A-C) Craniofacial fibrous dysplasia with left proptosis. Computed tomography MPR images show expansion of diploic space with ground-glass appearance (asterisk) involving hemifraniofacial bones on left. Note obliteration of sinuses, encroachment of orbit with overcrowding of orbital contents

## Conclusion

Multimodality approach for imaging of orbits helps in narrowing the differentials in establishing a confident radiologic diagnosis. CT is the modality of choice for bony detail and calcifications, whereas MR is superior for evaluation of the visual pathways, the globe and soft tissues. High resolution realtime USG, MDCT with valuable post-processing techniques and high field strength MRI are very useful in visualization of and characterization of orbital lesions. MRI DWI, MR spectroscopy, perfusion studies, Positron Emission Tomography (PET)-CT/MR has increasingly become important in the recent years, in evolving towards functional imaging.

## Acknowledgments

We express our sincere gratitude to our esteemed colleagues and the faculty of the Department of Radiodiagnosis, INHS Asvini for their valuable contributions and constant support.

## References

- Mafee MF. Orbit: Embryology, anatomy and pathology. In: Som PM, Curtin HD, editors. *Head and Neck Imaging*. 4<sup>th</sup> ed., vol. 2. St Louis: Mosby; 2003. p. 534-6.
- Aviv RI, Casselman J. Orbital imaging: Part 1. Normal anatomy. *Clin Radiol* 2005;60:279-87.
- Mafee MF, Putterman A, Valvassori GE, Campos M, Capek V. Orbital space-occupying lesions: Role of computed tomography and magnetic resonance imaging. An analysis of 145 cases. *Radiol Clin North Am* 1987;25:529-59.
- Aironi VD, Gandage SG. Pictorial essay: B-scan ultrasonography in ocular abnormalities. *Indian J Radiol Imaging* 2009;19:109-15.
- Rootman J. Distribution and differential diagnosis of orbital disease. In: *Diseases of the orbit: a multidisciplinary approach*. 2<sup>nd</sup> ed. Philadelphia, PA: Lippincott, Williams and Wilkins; 2003. p. 52-84.
- Dubey RB, Tara NP, Sisodiya KN. Computerised tomographic evaluation of orbital lesions: Pictorial essay. *Indian J Radiol Imaging* 2003;13:261-70.
- Eustis HS, Mafee MF, Walton C, Mondonca J. MR imaging and CT of orbital infections and complications in acute rhinosinusitis. *Radiol Clin North Am* 1998;36:1165-83.
- Weber AL, Romo LV, Sabates NR. Pseudotumor of the orbit. Clinical, pathologic, and radiologic evaluation. *Radiol Clin North Am* 1999;37:151-68.
- Flanders AE, Mafee MF, Rao VM, Choi KH. CT characteristics of orbital pseudotumors and other orbital inflammatory processes. *J Comput Assist Tomogr* 1989;13:40-7.
- Kirsch E, Hammer B, von Arx G. Graves' orbitopathy: Current imaging procedures. *Swiss Med Wkly* 2009;139:618-23.
- Dodds NI, Atcha AW, Birchall D, Jackson A. Use of high-resolution MRI of the optic nerve in Graves' ophthalmopathy. *Br J Radiol* 2009;82:541-4.
- Avery LL, Susaria SM, Novelline RA. Multidetector and Three-Dimensional CT Evaluation of the Patient With Maxillofacial Injury. *Radiol Clin North Am* 2011;49:183-203.
- Valvassori GE, Sabnis SS, Mafee RF, Brown MS, Putterman A. Imaging of orbital lymphoproliferative disorders. *Radiol Clin North Am* 1999;37:135-50.
- Flanders AE, Espinosa GA, Markiewicz DA, Howell DD. Orbital lymphoma. Role of CT and MRI. *Radiol Clin North Am* 1987;25:601-13.
- Shields JA. In: *Diagnosis and management of orbital tumors*. Philadelphia: WB Saunders; 1989. p. 149-69.
- Bilaniuk LT. Vascular lesions of the orbit in children. *Neuroimaging Clin N Am* 2005;15:107-20.
- Krohmel GB, Wright JE. Orbital hemorrhage. *Am J Ophthalmol* 1979;88:254-8.
- El Gammal T. MR of normal optic chiasm. *AJNR Am J Neuroradiol* 1991;12:584.
- Azar-Kia B, Naheedy MH, Elias DA, Mafee MF, Fine M. Optic nerve tumors: Role of magnetic resonance imaging and computed tomography. *Radiol Clin North Am* 1987;25:561-81.
- Mafee MF, Putterman A, Valvassori GE, Campos M, Capek V. Orbital space-occupying lesions: Role of computed tomography and magnetic resonance imaging. An analysis of 145 cases. *Radiol Clin North Am* 1987;25:529-59.
- Aviv RI, Miszkal K. Orbital imaging: Part 2. Intraorbital pathology. *Clin Radiol* 2005;60:288-307.
- Jackson A, Patankar T, Laitt RD. Intracranial optic nerve meningioma: A serious diagnostic pitfall. *AJNR Am J Neuroradiol* 2003;24:1167-70.
- Atlas SW. Magnetic resonance imaging of the orbit: Current status. *Magn Reson Q* 1989;5:39-96.
- Mafee MF, Goodwin J, Dorodi S. Optic nerve sheath meningiomas. Role of MR imaging. *Radiol Clin North Am* 1999;37:37-58.
- Weber AL, Mikulis DK. Inflammatory disorders of the paraorbital sinuses and their complications. *Radiol Clin North Am* 1987;25:615-30.
- Kapur R, Sepahdari AR, Mafee MF, Putterman AM, Aakalu V, Wendel LJ. MR Imaging of orbital inflammatory syndrome, Orbital Cellulitis, and Orbital Lymphoid Lesions: The Role of Diffusion-Weighted Imaging. *AJNR Am J Neuroradiol* 2009;30:64-70.
- Kaufman LM, Mafee MF, Song CD. Retinoblastoma and simulating lesions. Role of CT, MR imaging and use of Gd-DTPA contrast enhancement. *Radiol Clin North Am* 1998;36:1101-17.
- Mafee MF, Haik BG. Lacrimal gland and fossa lesions: Role of computed tomography. *Radiol Clin North Am* 1987;25:767-79.
- Mafee MF, Edward DP, Koeller KK, Dorodi S. Lacrimal gland tumors and simulating lesions. Clinicopathologic and MR imaging features. *Radiol Clin North Am* 1999;37:219-39.
- Grossman RI, Yousem DM. Orbit. In: *Neuroradiology: The Requisites*. 2<sup>nd</sup> ed. St Louis: Mosby; 2003. p. 469-516.
- Barnes L, Verbin R, Appel B, Peel R. Tumor and tumor like lesions of the soft tissue. In: Barnes L, editor. *Surgical Pathology of the Head and Neck*. 2<sup>nd</sup> ed., vol. 2. New York: Marcel Dekker; 2000. p. 1084-95.
- Khanna PC, Thapa MM, Iyer RS, Prasad SS. Pictorial essay: The many faces of craniosynostosis. *Indian J Radiol Imaging* 2011;21:49-56.

**Cite this article as:** Hande PC, Talwar I. Multimodality imaging of the orbit. *Indian J Radiol Imaging* 2012;22:227-39.

**Source of Support:** Nil, **Conflict of Interest:** None declared.